The equilibrium and fixed-bed study of malachite green adsorption on chitosan hydrogels

X. H. Song, K. L. Goh and K. Wang

ABSTRACT

Chitosan hydrogel beads were prepared by a precipitation process, and were used to investigate the adsorption of malachite green (MG) oxalate under various conditions. It was found that adsorption equilibrium was most sensitive to the pH value at pH <8 while fixed bed breakthrough kinetics presented asymmetric S-shaped profiles which could not be adequately described by conventional models such as Adams-Bohart and Yoon-Nelson. The possible reasons were discussed and an improved Adams-Bohart model was proposed to better describe the changes in mass transfer mechanisms during adsorption.

Key words | adsorption, breakthrough, chitosan, fixed bed, kinetics, malachite green

X. H. Song
School of Chemical & Biomedical Engineering,
Nanyang Technological University,
Singapore

K. L. Goh
Newcastle Research & Innovation,
Institute Pte Ltd (NewRIIS),
80 Jurong East Street 21, #05-04,
Singapore

K. Wang (corresponding author)
Department of Chemical Engineering,
Khalifa University of Science & Technology,
P.O. Box 2533, Abu Dhabi,
United Arab Emirates
and
Center for Catalysis and Separation
PO Box 127788, Abu Dhabi
United Arab Emirates
E-mail: *kean.wang@ku.ac.ae*

INTRODUCTION

Malachite green (MG) oxalate, a dark green and crystalline dye, has been widely used in the textile, paper and aquaculture industries (Crini 2006). Adsorption is a popular technology for dye removal from dye-containing waste water and is particularly attractive if the adsorbents are derived from abundant and low-cost sources. A large number of low-cost adsorbents have been reported; these absorbents fall under the following categories: polysaccharides (chitosan, cyclodextrin, starch, and their derivatives (Crini 2006; Crini *et al.* 2007), etc.); biomass/agricultural wastes (de-oiled soya (Mittal *et al.* 2005), sawdust/weeds (Malik *et al.* 2007; Tarawou & Horsfall Jr 2007), nut shells (Malik *et al.* 2007), etc.); minerals (clays (Cheknane *et al.* 2012), zeolites (Karadag *et al.* 2007), oxides (Muliwa *et al.* 2018)); activated carbons derived from waste tyres (Song *et al.* 2013); and sludge (Wang *et al.* 2008), etc.

Chitosan, the *N*-deacetylated derivative of chitin (poly (β-(1 → 4)-*N*-acetyl-D-glucosamine), is the second most abundant natural polymer after cellulose. It has excellent biodegradability, biocompatibility, non-toxicity, and good adsorption capacities (Li *et al.* 2008). For manufacturing purposes, chitosan may be molded into many desirable shapes, such as beads, filaments, and membranes. In water treatment, chitosan and its derivatives are widely used as low-cost adsorbents for the removal of heavy metals, dyes and other contaminants (Crini 2006; Li *et al.* 2008).

It is generally accepted that the amino groups of chitosan offer the main adsorption sites for metal ions and dyes. Amino groups are protonated under acidic conditions and show strong affinity to these molecules and ions (Xu *et al.* 2008). Chitosan hydrogel beads (grafted or crosslinked) have been a preferred choice because they have high specific surface area, more exposed free amino groups, and better porous networks for diffusion.

Several studies have been reported in the literature for MG adsorption on chitosan. For example, Bekci *et al.* (Bekçi *et al.* 2008) fabricated chitosan beads and studied MG adsorption in batch mode under different temperatures, pH ranges, and contact times. They found the MG adsorption involved a high activation energy of ~83 kJ/mol – implying a chemical process – with the highest adsorption capacity (~93 mg/g) occurring at the optimum pH of 8. The kinetics were seen to follow the second order rate.

Zheng *et al.* prepared composite hydrogels using chitosan, acrylic acid, itaconic acid, and attapulgite (Zheng *et al.* 2014). The hydrogel beads have an anionic surface and a 3D porous network, which present good adsorption capacity towards MG and dye mixtures. The maximum adsorption

doi: 10.2166/wst.2019.160

capacity was ~1,600 mg/g and the batch kinetics were seen to follow a pseudo second order rate (Zheng *et al.* 2014). Mittal *et al.* studied the adsorption kinetics of MG on de-oiled soya via batch and column experiments (Mittal *et al.* 2005). The batch kinetics were seen to follow a first order rate, while the column kinetics were found to be governed by external (film) transport at lower concentration and internal (pore) diffusion at high concentration (Mittal *et al.* 2005). Similar results were also found by the same group of researchers for MG adsorption on bottom ashes (Gupta *et al.* 2004).

To the best of our knowledge, there is a dearth of studies on the fixed bed kinetics of MG on chitosan. This could be attributed to the following factors. First, MG is a bulky basic dye; it forms dimers in solution so that the diffusion resistance is high. Second, during the MG adsorption process, the pH of the system can change from acidic (pH ~ 4) to basic (pH 7–10). The change in the acidity of the system will in turn change the protonation of the amine groups, the charge of the dye molecules and, consequently, affects the adsorption equilibrium as well as kinetics (Song *et al.* 2013).

A number of fixed bed studies have been reported for the adsorption of other dyes on chitosan, or MG on other adsorbents (Ahmed & Hameed 2018; Mohammad *et al.* 2018). For example, Xu *et al.* (Xu *et al.* 2008) studied the fixed bed kinetics of orange-7 on modified chitosan beads at high pH values. The breakthrough curves were found to be J-shaped which could be adequately modelled by the Wheeler-Jonas equation in a two-segmented approach (Xu *et al.* 2008). Chowdhury *et al.* (Chowdhury & Saha 2013) investigated the MG kinetics in a fixed bed column filled with the NaOH-modified rice husks. Among the four breakthrough models (namely Adams-Bohart, bed depth service time, Thomas, and Yoon-Nelson), the Thomas model provided the line of best fit to the breakthrough curves (Chowdhury & Saha 2013). Cheknane *et al.* studied the fixed bed kinetics of MG on granular pillared clays and found that the kinetics were significantly affected by the particle size, bed height, and operation parameters (Cheknane *et al.* 2012). Two models (Clark and Yoon-Nelson) were used to evaluate the breakthrough kinetics; it was found that the Clark model provided the line of best fit to the breakthrough data (Cheknane *et al.* 2012). Vieira *et al.* (Vieira *et al.* 2018) studied the fixed bed kinetics of azo dye on chitosan adsorbents with different deacetylation degrees and found that the breakthrough curves predicted by the Thomas and Yoon-Nelson models were in good agreement with experimental results, particularly at the higher outlet concentrations. In a study on an anionic dye (methyl orange (MO)) adsorption on macroporous alginate/ferrihydrite beads, the fixed bed breakthrough curves predicted by the Thomas model were in good agreement with experimental results (Zhao *et al.* 2017).

The continuously operated fixed bed column is a preferred option to a batch adsorber for industry applications. There is an abundant literature on the mathematical modelling of fixed bed breakthrough kinetics. These models range from the complicated heterogeneous multiple-phase models (fluid, pore, surface) (Lv *et al.* 2008) to the simplified single-phase models such as the Adams-Bohart, Thomas, and Yoon-Nelson models mentioned in previous paragraph, as well as the bed depth service time (BDST) and Wheeler models (Chowdhury & Saha 2013). The single-phase models have been extensively used in the study of biosorption processes (Tien 2007; Chu 2010; Chowdhury & Saha 2013). The main purpose of this report is to investigate the MG adsorption kinetics on chitosan hydrogels in a fixed bed evaluated using the conventional models, namely Adams-Bohart, Thomas, and Yoon-Nelson, as well as a modified Adams-Bohart model.

THEORIES

For practical applications, the fixed bed breakthrough model should closely reflect the mass transfer and flow conditions in the real system in the most straightforward way. The single phase model proposed by Bohart and Adams (Bohart & Adams 1920), which assumes that the adsorption rate is proportional to the residual capacity of the adsorbent and the concentration of the adsorbing species, has been widely used to study the column kinetics of biosorption of dyes and metal ions (Gupta *et al.* 2004; Cheknane *et al.* 2012; Chowdhury & Saha 2012, 2013). The simplified linearized form of this model is shown in Equation (1):

$$ln\left(\frac{C_0}{C_t}-1\right)=\frac{KN_0Z}{U_0}-KC_0t \quad (1)$$

where C_0 and C_t are the influent and effluent concentrations (ml/L), respectively, Z is the bed height (cm), U_0 is the linear velocity (cm/min), K is the rate constant (L/mg/min), and N_0 is the volume adsorption capacity (mg/L). The model constants (K and N_0) can be determined from the plot of $\ln[(C_0/C_t)-1]$ against time (t) for given values of flow rate and bed height. This model is known for its accuracy in predicting the initial stage (i.e. $C_t/C_0 \sim 0.10$) of the breakthrough curve. The re-arrangement of Equation (1) in term of time generates the BDST model, which is simply a variant of the Adams-Bohart model and has been used to evaluate a wide range of C_t/C_0 values, i.e. up to 0.50 (Chu 2010; Sotelo

et al. 2013). Another equally popular model is the Thomas model, which takes the linearized form of:

$$ln\left(\frac{C_0}{C_t}-1\right)=\frac{K_T q_0 M}{Q}-K_T C_0 t \quad (2)$$

where K_T is the rate constant, q_0 is the sorption capacity of adsorbent per unit mass, M is the mass of adsorbent and Q is the flow rate. Chu had pointed out that Adams-Bohart model assumes a rectangular isotherm with a quasi-chemical rate expression, whereas the Thomas model assumes a Langmuir isotherm with a pseudo second order rate in the original model development (Chu 2010). The two models are equivalent to each other under a highly favorable isotherm (Chu 2010). For the simple purpose of curve-fitting of the breakthrough data, Equations (1) and (2) are equivalent in performance and should not be used separately.

The Yoon-Nelson model (Yoon & Nelson 1984) is widely used for evaluated empirical results owing to its simplicity. The model takes the linearized form of:

$$ln\left[\frac{C_t}{C_0-C_t}\right]=k(t-\tau) \quad (3)$$

where k is the reaction constant (s^{-1}), and τ is the time required for retaining 50% adsorbate in the feed (or a complete bed saturation at $t=2\tau$). Here, the two models, namely Equations (1) and (3), are examined to investigate their capability for simulating the kinetics of MG adsorption in a fixed bed column.

EXPERIMENTAL

Materials and preparation

MG (malachite green, $C_{52}H_{54}N_4O_{12}$, CI 42,000, with a purity greater than 80%) was supplied by Sigma-Aldrich. A stock solution containing 1,000 ppm was prepared by dissolving 500.00 mg of MG in 500 mL of deionised (DI) water. Chitosan was purchased from Bioline Company; the degree of deacetylation was greater than 90%. To make chitosan hydrogel beads, 2.0 g of chitosan powder were dissolved in 100 ml of 1% acetic acid solution (V/V). The mixture solution was stirred overnight, filtered, and then pumped through a syringe needle (27 G) into 1 M of NaOH solution, and stirred until spherical hydrogel beads had formed. The beads were filtered and neutralized by rinsing with tap water, followed by ethanol and DI water. The beads were freeze dried prior to analysis. Further details concerning the preparation process are available elsewhere (Li et al. 2008; Xu et al. 2008; Song et al. 2012).

Batch and column experiments

About 100 mg of blot-dried beads (a dosage of ~2 g/L) was added to the dye solution in conical flasks. The mixture was stirred at 200 rpm in a shaker at room temperature. The pH values of the MG solutions were adjusted by adding 0.5 M of NaOH to maintain pH ~7.5. Liquid samples were withdrawn from the solution for analysis over the next 72 hours. The concentrations of the sample solutions were analyzed using a UV visible spectrophotometer at $\lambda_{max}=667$ nm. The amount of MG adsorbed onto the adsorbent, q_e (mg/g), was calculated according to the following equation:

$$q_e=(C_0-C_e)\frac{V}{m} \quad (4)$$

where C_0 and C_e (mg/L) are the initial and equilibrium concentrations of MG, respectively, V (ml) is the solution volume, and m (g) is the mass of adsorbent.

The fixed bed kinetics were measured in a glass column with a diameter of 2.5 cm and a length of 25 cm. Chitosan hydrogel beads of a given mass and packing volume were placed in the column filled with water. Quartz fibers were fixed as the filters at the inlet/outlet.

Figure 1 shows the schematic diagram of the breakthrough experiment. An influent MG solution was continuously fed into the column by a peristaltic pump in a down-flow mode. At a fixed time interval, the effluent

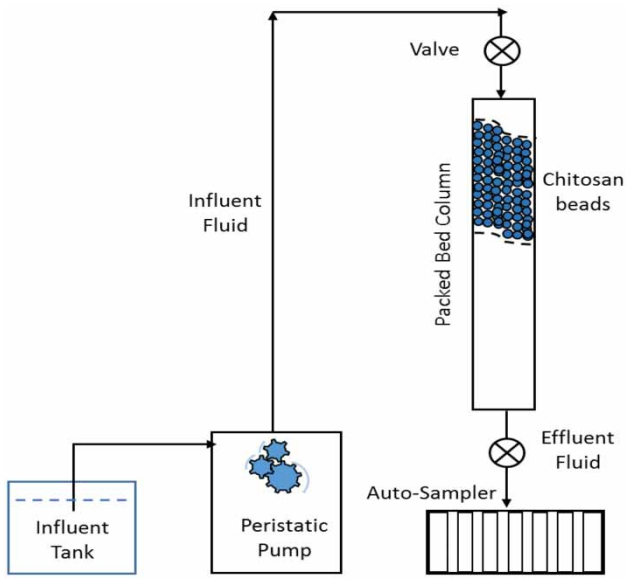

Figure 1 | The schematic diagram of the fixed bed experiment.

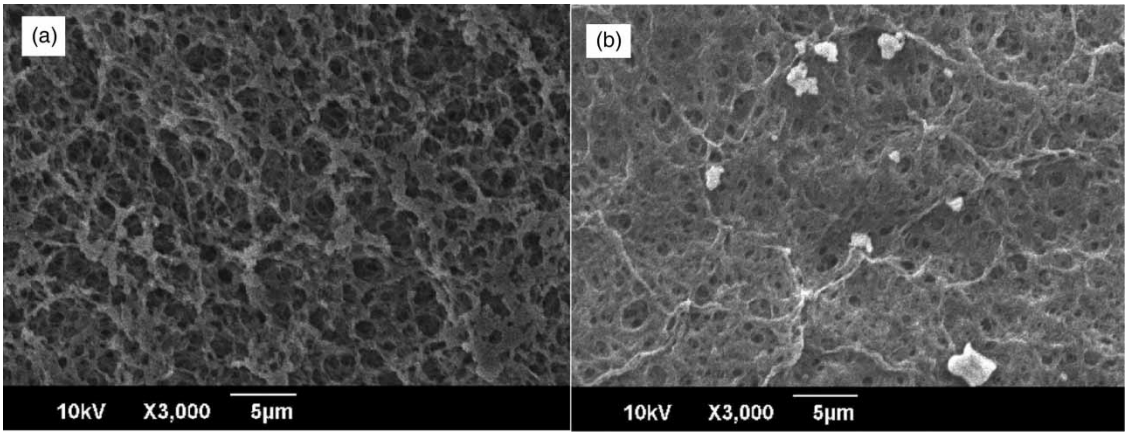

Figure 2 | SEM micrographs of chitosan beads (a) before adsorption, and (b) after adsorption of MG.

was collected by the auto-sampler and analyzed by UV spectrometer. The breakthrough and bed exhaustion time were identified as corresponding to the ratio of the concentrations of effluent to influent at 5% and 95%, respectively.

Scanning electron microscopy

The morphology of the chitosan beads was examined using a high-resolution JEOL JSM-6390LA field-emission scanning electron microscope (SEM). SEM micrographs of the specimens were acquired for native and MG adsorbed beads, respectively.

Fourier-transform infrared spectroscopy

Spectra from a Fourier transform infrared spectroscopy (FTIR) spectrometer (FTS3100, Varian Inc., USA) were obtained for both the native and MG adsorbed chitosan beads. Approximately 2 mg of each sample was embedded in 100 mg KBr and the mixture was pressed into disc samples. The FTIR sample compartment was continuously purged with dry air to prevent the formation of water vapor. All spectra were obtained from 600 to 4,000 cm^{-1} with 36 scans per specimen, at 4 cm^{-1} resolution, and averaged to obtain a representative plot. Background subtraction was carried out by software.

RESULTS AND DISCUSSION

Characterization

SEM

SEM micrographs of freeze-dried beads were shown in Figure 2. It can be observed in Figure 2(a) that the dry native beads are highly macroporous, with the pore diameter of ~200–1,000 nm, estimated using software ImageJ (Yang *et al.* 2018); these pores provide channels for diffusion into the inner surface. After MG adsorption (Figure 2(b)), the surface of the beads appears smoother and particles (the light spots) varying in size from 500 nm to 2 μm, can be observed. These particles are attributed to the formation of MG salts or residue (crystals) as a result of freeze drying.

BET analysis

Table 1 lists the surface characteristics of the freeze-dried native beads analyzed by the standard N_2 isotherm at 77 K. The results reveal that the beads are highly macroporous, with an average specific surface area of 53 m^2/g. This is consistent with other research (Marrakchi *et al.* 2016), which shows that the mechanisms of dye adsorption on chitosan and its derivatives are predominantly chemical adsorption rather than physical adsorption, which is dependent on the surface area.

FTIR

Figure 3 shows the FTIR spectra of the native and MG-adsorbed beads. Comparative analysis reveals that the bands at 1,650.5 cm^{-1} and 1,590.8 cm^{-1} (–NH bending vibration in $–NH_2$) have shifted to 1,644.2 cm^{-1} and

Table 1 | Surface characteristics of chitosan beads (freeze dried)

Average bead diameter (mm)	~2
BET surface area (m^2/g)	53
Total pore volume (cm^3/g)	0.06 for pores smaller than 40 nm
Porosity	0.63

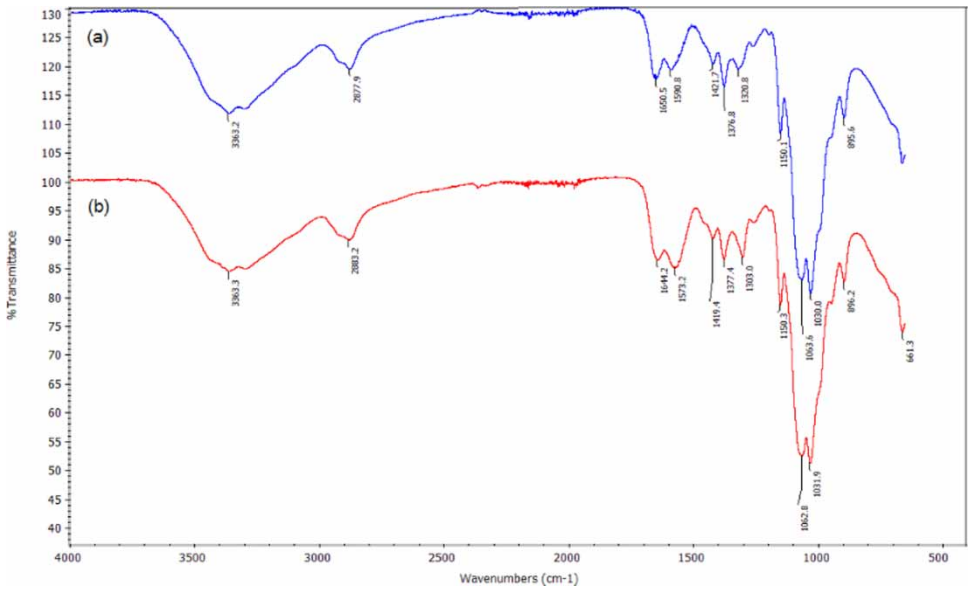

Figure 3 | FTIR spectra of (a) native chitosan beads, and (b) MG adsorbed beads.

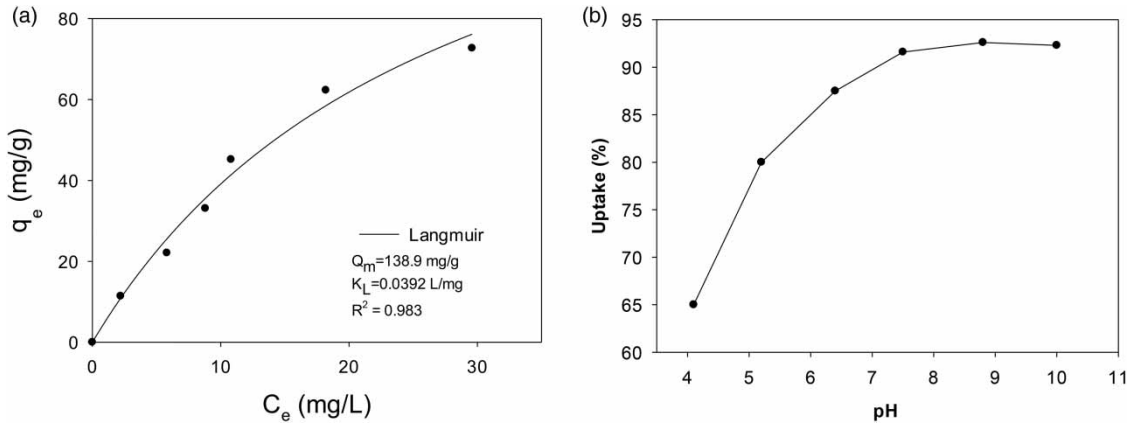

Figure 4 | Characteristic curves of MG adsorption on chitosan: (a) MG isotherm data (dots) obtained from chitosan beads (pH ~ 7.5), and the line of best fit using the Langmuir equation, (b) effects of pH on MG adsorption by chitosan beads.

1,573.2 cm^{-1}, respectively, and the band intensity at 1,573.2 cm^{-1} has increased due to the weak interaction of MG with chitosan. There was no significant change in band intensity at wavenumbers of 3,359.6 cm^{-1} (–OH and –NH overlapping stretching vibration), 1,376 cm^{-1} (–CH symmetric blending vibration in –CHOH–), 1,320.8 cm^{-1} (–CN stretching vibration), 1,421.7 cm^{-1} (–NH deformation vibration in $–NH_2$), 1,150.1 cm^{-1} (–CN stretching vibration), and 896.6 cm^{-1} (–CN stretching vibration). These observations imply that the adsorbed MG (in dry mode) was predominantly in a physical adsorption mode – no chemical reaction was implied. Similar observations have also been reported elsewhere (Azlan *et al.* 2009).

Adsorption isotherm

Figure 4(a) shows the MG adsorption data and the line of best fit using the Langmuir isotherm equation, i.e.

$$q_e = Q_m K_L C_e/(1 + K_L C_e) \quad (5)$$

where K_L is the affinity (L/mg) and C_e, q_e, and Q_m are the liquid phase concentration, adsorbed phase concentration, and maximum adsorption capacity, respectively. The isotherm parameters and the goodness-of-fit ($R^2 \sim 0.98$) are listed in the legend of Figure 4(a). These results indicate that the MG adsorption is characterized by a typical type-I

isotherm underpinning a monolayer adsorption mechanism (Debrassi *et al.* 2012).

The effect of pH on MG uptake was studied as follows: 0.15 g of chitosan beads was introduced into 50 ml of MG solution (with a concentration of 40 ppm) and the pH of the dye solution was adjusted using 0.1 M of NaOH solution. The results are shown in Figure 4(b); it can be observed that the uptake increases from 65% to 92.3% when the pH value increases from 4 to 10. The MG adsorption is strongly pH dependent at pH <8 but gradually settles at a stable uptake value at high pH values (pH >8).

Since the pKa value of chitosan is ~6.3 (Li *et al.* 2008), the amino groups of chitosan are protonated at pH values of less than 6. This will repulse the cationic dye in acidic solutions and result in a low MG uptake. At basic conditions, however, the chitosan surface is negatively charged and this could greatly enhance the MG adsorption (Song *et al.* 2013). Similar behaviours were also reported by other researchers (Bekçi *et al.* 2008; Debrassi *et al.* 2012).

Fixed bed experiments

Figure 5(a) presents the MG breakthrough kinetic curves (symbols) in the fixed bed filled with chitosan hydrogels. The feed contained 10 ppm MG solution at the pH of 7.5. The breakthrough curves correspond to the following volumetric feed rates of 0.97, 2.09, 3.15, and 4.95 ml/min. The breakthrough kinetics are presented as the ratio of the concentration of effluent to feed (C_t/C_0) versus time. The results show that increasing the feed rate from 0.97 to 4.95 ml/min decreases the breakthrough time (t_b) from 60 min to 10 min; consequently this results in steep breakthrough curves.

The linear plots of the breakthrough data using the Adams-Bohart model (Equation (1)) and the Yoon-Nelson model (Equation (3)) are shown in Figure 6(a) and 6(b), respectively. Software MS Excel was used to carry out the

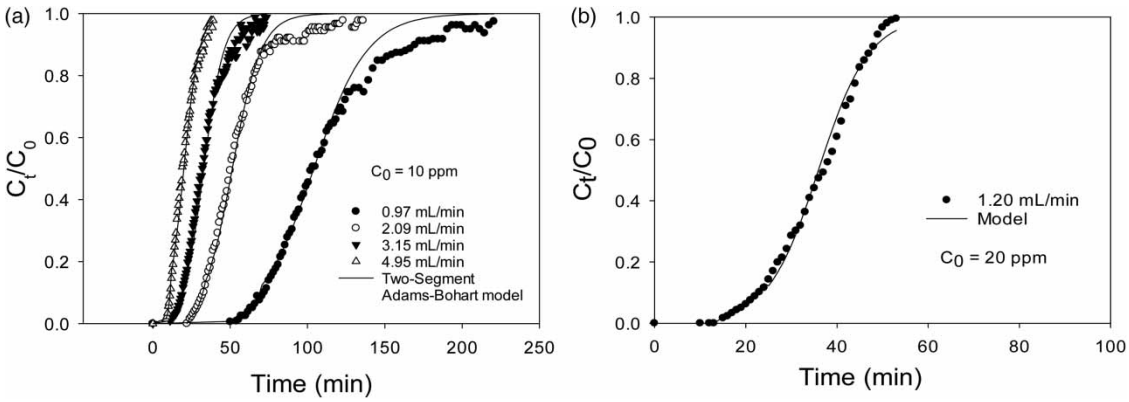

Figure 5 | Breakthrough curves of MG adsorption on chitosan hydrogels at (a) $C_0 = 10$ ppm; (b) $C_0 = 20$ ppm. The two-segment Adams-Bohart model was used to fit the experimental data.

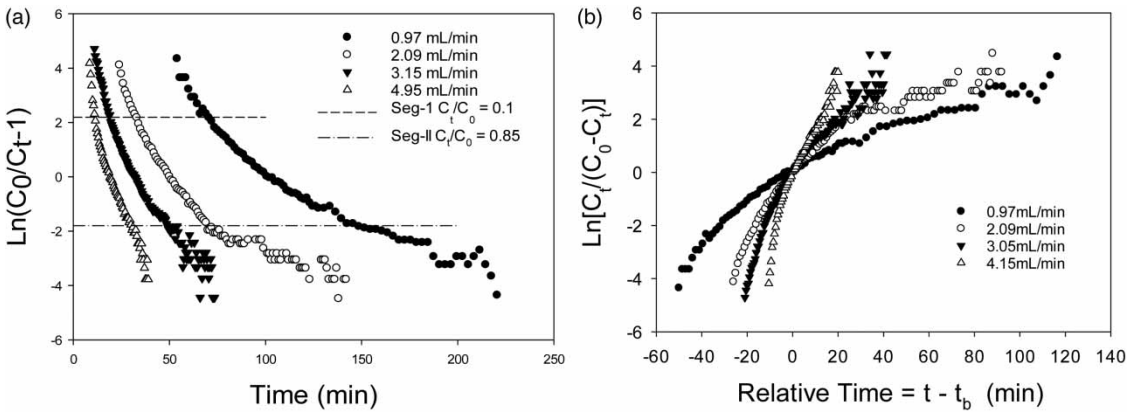

Figure 6 | The linear plots of kinetic data. (a) Adams-Bohart model ($R^2 = 0.92, 0.86, 0.94, 0.95$) and (b) Yoon-Nelson model ($R^2 = 0.89, 0.85, 0.94, 0.95$).

linear regression analysis and generate the linear plots. The values of the goodness-of-fit (R^2) for each set of breakthrough data are listed in the captions. At high flow rates, all models describe the breakthrough kinetics very well ($R^2 \sim 0.95$). However, at low flow rates, all models yield lower R^2 values – in particular, the Yoon-Nelson model gives and $R^2 = 0.85$.

A technical discussion of possible reasons for the discrepancy between the breakthrough data of MG and the traditional models is now presented in light of findings from many studies that have shown otherwise (Tien 2007). From the mathematical perspective, the Yoon-Nelson model features only one fitting parameter while the Adams-Bohart model features two independent fitting parameters. Thus, it is not surprising that the Yoon-Nelson model could not fit the breakthrough data adequately. From the physical perspective, all models share several simplifying assumptions, namely: plug flow, surface reaction control, homogeneous adsorbents, and symmetric breakthrough curves, but these simplifying assumptions may be inconsistent with the reality of the fixed bed process (Xu *et al.* 2008; Chu 2010).

Axial dispersion can be significant compared to bulk flow under laminar flow, which contribute partially to the nonlinearity of the plotted data at the low flow rate (Reynolds number (R_e) ~ 1 at the feed rate of 0.97 ml/min or a superficial velocity of 0.20 cm/min). As the flow rate increases, the effect of axial dispersion reduces progressively, which explains the improved linearity at the high flow rate ($R_e \sim 4$ at the feed rate of 4.95 mL/min).

The diffusion barrier and surface heterogeneity may also contribute to the discrepancy between the model and the breakthrough data. The MG is a bulky molecule with size of 1.2 nm × 1.2 nm × 0.57 nm (Song *et al.* 2013). The shape of the breakthrough curve corresponds to the mass transfer zone (MTZ) in the fixed bed, in which MG molecules are gradually adsorbed onto the fresh chitosan surface. The initial rate of adsorption is faster on the clean and exposed sites of chitosan, in which the film resistance plays a major part. The subsequent diffusion into the inner surface of chitosan matrix, however, could result in significant diffusion resistance. This slower pore/surface diffusion will play a dominant role in the overall kinetics. Meanwhile, the pH of the solution also changes progressively in the MTZ, which subsequently alters the driving force for MG adsorption.

The complicated mass transfer mechanisms have also been observed by other researchers. For instance, Mittal *et al.* observed a rate-limiting step in the change from external film diffusion at low concentration to internal pore diffusion at high concentration in the biosorption of MG (Mittal *et al.* 2005). Chu and Hashim demonstrated the inability of the Adams-Bohart model to predict the asymmetric breakthrough kinetics in the biosorption of metal ions (Chu & Hashim 2007).

For practical applications, it is desirable to have a model which can account for the complex mass transfer mechanism in a 'lumped' approach. In this study, we propose to use the two-segmented approach, which has been successfully applied to model the J-shaped breakthrough curves of Orange-7 on modified chitosan beads (Xu *et al.* 2008). This approach is suitable for the Adams-Bohart model as it is more applicable to the initial stage of the breakthrough curve ($C_t/C_0 < 0.10$) (Quintelas *et al.* 2008; Chu 2010; Chowdhury & Saha 2013), which approximately characterizes the turning point of the linear plots in Figure 6(a). The Yoon-Nelson model would not be suitable for two reasons: (1) the constraint of the single parameter and (2) the ambiguity of the mechanisms underpinning the model.

The proposed two-segment approach was then applied to the breakthrough data in Figure 6, in which the Adams-Bohart model (which is a variant of the Thomas model) was used to fit the data in each segment separately. Yoon-Nelson's model was not further tested because it exhibited reduced linearity at the lower as well as higher concentration regions (Figure 6(b)), due to the constraints imposed on the model. The first segment (S1) corresponds to values of C_t/C_0 from 0 to 0.10 (the dashed line in Figure 6(a)) while the second segment (S2) corresponds to values of C_t/C_0 from 0.10 to 0.85 (the dash-dotted line). The data of high concentration ($C_t/C_0 > 0.85$) were not evaluated because they show a wide scatter, and they are located near the bed exhaustion point.

Table 2 lists the linear regression results of the two-segmented Adams-Bohart model evaluated using MS Excel. Of note, in all cases the R^2 is greater than 0.95; in comparison, the conventional Adams-Bohart model yields an R^2 value which is equal to or lower than 0.95 (Figure 6(a)). This indicates that the two-segmented model is a better approach for describing the breakthrough data. In all cases, the rate constants (i.e. K) of S1 are higher than S2. In general, as the flow velocity (U_0) increases from 0.20 to 0.85, the rate constants of S1 increase more dramatically (≥3 times) than that of S2 (about twice). Also of note is the fact that the bed capacity (N_0) is relatively stable in each segment; numerically, the value of the N_0 corresponding to S2 is generally two-fold higher than that of S1.

The good agreement between the modified Adams-Bohart model (based on the two-segmented approach) and

Table 2 | Optimal parameters of the two-segmented Adams-Bohart model

			K (L·min/mg)		N_0 (mg/L)		R^2	
Feed concentration (ppm)	**Q (ml/min)**	**U_0 (cm/min)**	**S1**	**S2**	**S1**	**S2**	**S1**	**S2**
10	0.97	0.198	0.0182	0.0058	2.25	8.92	0.94	0.98
10	2.09	0.426	0.0209	0.0107	5.27	9.51	0.98	0.97
10	3.15	0.622	0.0313	0.0152	4.36	8.89	0.96	0.96
10	4.95	0.846	0.0714	0.0200	5.20	7.36	0.98	0.98
20	1.20	0.240	0.0111	0.0090	7.13	8.80	0.98	0.97

the breakthrough kinetics of the MG adsorption on chitosan beads are consistent with our previous analyses. The two-segmented approach is expected to have wide applicability in biosorption processes with the Adams-Bohart and other two-parameter kinetic models. In principle, the two-segmented approach underpins two distinct adsorption sites, namely the outer and inner surfaces of the porous network in chitosan. As the diffusion front of the MTZ travels through the fixed bed, the adsorption rate is faster on the fresh chitosan surface on which the overall kinetic rate is controlled by the film resistance (S1). Therefore, the rate constant is more sensitive to the flow rate in this segment. The subsequent MG diffusion into the inner surface of the chitosan hydrogels will experience a significant diffusion barrier and is largely limited by the pore diffusion (S2), with the driving force being affected by the variation in pH values as well. The variation in the derived bed capacity value (N_0) suggests that more adsorption sites are available as pore diffusion occurs in the inner surface.

The sensitivity of the two-segmented Adams-Bohart model is investigated further by fitting the model to the breakthrough data measured at a higher feed concentration ($C_0 = 20$ ppm), and at a different flow rate of 1.20 mL/min. Figure 5(b) shows the breakthrough data (dots) and the fitting of the two-segmented Adams-Bohart model (line). The parameters derived from the fitting are also listed in the last row of Table 2. The model is in good agreement with the breakthrough data ($R^2 \sim 0.98$) while the value of K optimally obtained at $C_0 = 20$ ppm is of the same order of magnitude as that obtained at $C_0 = 10$ ppm for the flow rate of 0.97 mL/min.

CONCLUSION

Chitosan hydrogel is an efficient adsorbent for the separation of MG from aqueous solution. The adsorption process is predominantly pH-dependent at pH <8 with slow kinetics. The fixed bed breakthrough curves are asymmetric in general, which cannot be described by such conventional models as Adams-Bohart, Thomas, or Yoon-Nelson, because of the complicated mass transfer mechanisms during the biosorption process. However, the modified Adams-Bohart model, based on a two-segmented approach to account for the changes in the mass transfer mechanisms during adsorption, yields excellent fitting and predictive capability to the breakthrough data over different operating conditions of the biosorption process.

ACKNOWLEDGEMENT

This project is based on the work partially supported by Khalifa University under Award No. RCII-2018-024.

REFERENCES

Ahmed, M. J. & Hameed, B. H. 2018 Removal of emerging pharmaceutical contaminants by adsorption in a fixed-bed column: a review. *Ecotoxicology and Environmental Safety* **149**, 257–266.

Azlan, K., Wan Saime, W. N. & Lai Ken, L. 2009 Chitosan and chemically modified chitosan beads for acid dyes sorption. *Journal of Environmental Sciences* **21** (3), 296–302.

Bekçi, Z., Özveri, C., Seki, Y. & Yurdakoç, K. 2008 Sorption of malachite green on chitosan bead. *Journal of Hazardous Materials* **154** (1–3), 254–261.

Bohart, G. & Adams, E. 1920 Some aspects of the behavior of charcoal with respect to chlorine. 1. *Journal of the American Chemical Society* **42** (3), 523–544.

Cheknane, B., Baudu, M., Basly, J.-P., Bouras, O. & Zermane, F. 2012 Modeling of basic green 4 dynamic sorption onto granular organo-inorgano pillared clays (GOICs) in column reactor. *Chemical Engineering Journal* **209**, 7–12.

Chowdhury, S. & Saha, P. D. 2012 Fixed-bed adsorption of Malachite Green onto binary solid mixture of adsorbents: seashells and eggshells. *Toxicological and Environmental Chemistry* **94** (7), 1272–1282.

Chowdhury, S. & Saha, P. D. 2013 Adsorption of malachite green from aqueous solution by NaOH-modified rice husk: fixed-bed column studies. *Environmental Progress and Sustainable Energy* **32** (3), 633–639.

Chu, K. H. 2010 Fixed bed sorption: setting the record straight on the Bohart–Adams and Thomas models. *Journal of Hazardous Materials* **177** (1), 1006–1012.

Chu, K. & Hashim, M. 2007 Copper biosorption on immobilized seaweed biomass: column breakthrough characteristics. *Journal of Environmental Sciences* **19** (8), 928–932.

Crini, G. 2006 Non-conventional low-cost adsorbents for dye removal: a review. *Bioresource Technology* **97** (9), 1061–1085.

Crini, G., Peindy, H. N., Gimbert, F. & Robert, C. 2007 Removal of C.I. Basic Green 4 (Malachite Green) from aqueous solutions by adsorption using cyclodextrin-based adsorbent: kinetic and equilibrium studies. *Separation and Purification Technology* **53** (1), 97–110.

Debrassi, A., Corrêa, A. F., Baccarin, T., Nedelko, N., Ślawska-Waniewska, A., Sobczak, K., Dłużewski, P., Greneche, J.-M. & Rodrigues, C. A. 2012 Removal of cationic dyes from aqueous solutions using *N*-benzyl-*O*-carboxymethylchitosan magnetic nanoparticles. *Chemical Engineering Journal* **183** (0), 284–293.

Gupta, V. K., Mittal, A., Krishnan, L. & Gajbe, V. 2004 Adsorption kinetics and column operations for the removal and recovery of malachite green from wastewater using bottom ash. *Separation and Purification Technology* **40** (1), 87–96.

Karadag, D., Turan, M., Akgul, E., Tok, S. & Faki, A. 2007 Adsorption equilibrium and kinetics of reactive black 5 and reactive red 239 in aqueous solution onto surfactant-modified zeolite. *Journal of Chemical & Engineering Data* **52** (5), 1615–1620.

Li, C. B., Hein, S. & Wang, K. 2008 Biosorption of chitin and chitosan. *Materials Science and Technology* **24** (9), 1088–1099.

Lv, L., Zhang, Y., Wang, K., Ray, A. K. & Zhao, X. S. 2008 Modeling of the adsorption breakthrough behaviors of Pb^{2+} in a fixed bed of ETS-10 adsorbent. *Journal of Colloid and Interface Science* **325** (1), 57–63.

Malik, R., Ramteke, D. S. & Wate, S. R. 2007 Adsorption of malachite green on groundnut shell waste based powdered activated carbon. *Waste Management* **27** (9), 1129–1138.

Marrakchi, F., Khanday, W. A., Asif, M. & Hameed, B. H. 2016 Cross-linked chitosan/sepiolite composite for the adsorption of methylene blue and reactive orange 16. *International Journal of Biological Macromolecules* **93**, 1231–1239.

Mittal, A., Krishnan, L. & Gupta, V. K. 2005 Removal and recovery of malachite green from wastewater using an agricultural waste material, de-oiled soya. *Separation and Purification Technology* **43** (2), 125–133.

Mohammad, M., Maitra, S. & Dutta, B. K. 2018 Comparison of activated carbon and physic seed hull for the removal of malachite green dye from aqueous solution. *Water, Air, & Soil Pollution* **229** (45), 1–14.

Muliwa, A. M., Leswifi, T. Y., Maity, A., Ochieng, A. & Onyango, M. S. 2018 Fixed-bed operation for manganese removal from water using chitosan/bentonite/MnO composite beads. *Environmental Science and Pollution Research* **25** (18), 18081–18095.

Quintelas, C., Fernandes, B., Castro, J., Figueiredo, H. & Tavares, T. 2008 Biosorption of Cr (VI) by three different bacterial species supported on granular activated carbon – a comparative study. *Journal of Hazardous Materials* **153** (1), 799–809.

Song, X., Li, C., Xu, R. & Wang, K. 2012 Molecular-ion-imprinted chitosan hydrogels for the selective adsorption of silver(I) in aqueous solution. *Industrial & Engineering Chemistry Research* **51** (34), 11261–5.

Song, X., Xu, R. & Wang, K. 2013 High capacity adsorption of malachite green in a mesoporous tyre-derived activated carbon. *Asia-Pacific Journal of Chemical Engineering* **8** (1), 172–177.

Sotelo, J. L., Ovejero, G., Rodriguez, A., Alvarez, S. & Garcia, J. 2013 Adsorption of carbamazepine in fixed bed columns: experimental and modeling studies. *Separation Science and Technology* **48** (17), 2626–2637.

Tarawou, T. & Horsfall Jr, M. 2007 Adsorption of methylene blue dye on pure and carbonized water weeds. *Bioremediation Journal* **11** (2), 77–84.

Tien, C. 2007 Remarks on adsorption manuscripts received and declined: an editorial. *Separation and Purification Technology* **54** (3), 277–278.

Vieira, M. L. G., Martinez, M. S., Santos, G. B., Dotto, G. L. & Pinto, L. A. A. 2018 Azo dyes adsorption in fixed bed column packed with different deacetylation degrees chitosan coated glass beads. *Journal of Environmental Chemical Engineering* **6** (2), 3233–3241.

Wang, X., Zhu, N. & Yin, B. 2008 Preparation of sludge-based activated carbon and its application in dye wastewater treatment. *Journal of Hazardous Materials* **153** (1–2), 22–27.

Xu, D., Hein, S., Loo, S. L. & Wang, K. 2008 The fixed-bed study of dye removal on chitosan beads at high pH. *Industrial & Engineering Chemistry Research* **47** (22), 8796–8800.

Yang, Y., Raza, A., Banat, F. & Wang, K. 2018 The separation of oil in water (O/W) emulsions using polyether sulfone & nitrocellulose microfiltration membranes. *Journal of Water Process Engineering* **25**, 113–117.

Yoon, Y. H. & Nelson, J. H. 1984 Application of gas adsorption kinetics I. A theoretical model for respirator cartridge service life. *The American Industrial Hygiene Association Journal* **45** (8), 509–516.

Zhao, L., Basly, J.-P. & Baudu, M. 2017 Macroporous alginate/ferrihydrite hybrid beads used to remove anionic dye in batch and fixed-bed reactors. *Journal of the Taiwan Institute of Chemical Engineers* **74**, 129–135.

Zheng, Y., Zhu, Y. & Wang, A. 2014 Highly efficient and selective adsorption of malachite green onto granular composite hydrogel. *Chemical Engineering Journal* **257**, 66–73.

First received 12 October 2018; accepted in revised form 25 April 2019. Available online 6 May 2019